A calibration-free ammonia breath sensor using a quantum cascade laser with WMS 2f/1f

Kyle Owen · Aamir Farooq

Abstract The amount of ammonia in exhaled breath has been linked to a variety of adverse medical conditions, including chronic kidney disease (CKD). The development of accurate, reliable breath sensors has the potential to improve medical care. Wavelength modulation spectroscopy with second harmonic normalized by the first harmonic (WMS 2f/1f) is a sensitive technique used in the development of calibration-free sensors. An ammonia gas sensor is designed and developed that uses a quantum cascade laser operating near 1,103.44 cm^{-1} and a multipass cell with an effective path length of 76.45 m. The sensor has a 7 ppbv detection limit and 5 % total uncertainty for breath measurements. The sensor was successfully used to detect ammonia in exhaled breath and compare healthy patients to patients diagnosed with CKD.

1 Introduction

The medical significance of the presence of ammonia in breath has been studied previously, demonstrating the usefulness of an ammonia sensor to diagnose and monitor a variety of medical conditions, including chronic kidney disease (CKD) [1], Helicobacter pylori infection [2], and encephalopathy [3]. Ammonia is a naturally occurring species in exhaled breath. Healthy individuals typically have a few hundred parts per billion by volume (ppbv) ammonia in their breath, while patients diagnosed with

K. Owen · A. Farooq (✉)
Clean Combustion Research Center, Division of Physical Sciences and Engineering, King Abdullah University of Science and Technology (KAUST), Thuwal 23955-6900, Saudi Arabia
e-mail: Aamir.Farooq@kaust.edu.sa

K. Owen
e-mail: kyle.owen@kaust.edu.sa

CKD, for example, could have over one part per million by volume (ppmv) ammonia in their breath [4]. Based on the established link between ammonia breath concentration and adverse medical conditions, the development of accurate sensors can improve medical treatment, providing beneficial diagnostic and monitoring tools. Laser-based sensors show great potential as they can achieve high sensitivity, provide real-time analysis, and their size makes them portable.

Table 1 summarizes recent developments in laser-based ammonia breath sensors as well as the sensor developed in this work. All of these sensors were developed using strong absorption features in ammonia's v_2 vibrational band, seen in Fig. 1. Carbon dioxide and water vapor, typically found in exhaled breath to be about 5 % and 6 % of the total gas mixture, respectively, also absorb in this wavelength region. The sensors described in Table 1 utilize strong ammonia transitions that have minimal interference from carbon dioxide and water vapor. The absorption feature near 1,103.44 cm^{-1} was chosen for this work because it has the least interference; <1 % of the absorbance at the ammonia peak is due to absorption from other species. Figure 2 shows a comparison between three ammonia absorption features and the interference from carbon dioxide and water vapor.

This is the first ammonia breath sensor developed using this low interference feature; however, an ammonia sensor for atmospheric measurements using the same feature has been developed previously [9]. Our sensor is also unique in that it is calibration free and therefore does not require a reference cell or a correlation based on previous calibration experiments. The WMS 2f/1f method enables calibration-free detection as long as the spectroscopic parameters of the absorption feature are known. These parameters are typically taken from the HITRAN database [8]; however, breath composition is different from air so the broadening

Table 1 Summary of recent laser-based ammonia breath sensors and the sensor developed in this work

Frequency	Laser	Method	Calibration	Interference (%)[a]	Reported Sensitivity[b]	References
Discrete lines 9–10 μm	CO_2	PAS	Reference cell		10 % for breath measurements as low as 100 ppbv	[1]
967.35 cm^{-1}	QCL	Pulsed CRDS	Calibration curve	4.55	50 ppbv detection limit	[4]
1,046.4 cm^{-1}	QCL	QEPAS	Reference cell	7.27	20 ppbv standard deviation	[5]
967.35 cm^{-1}	QCL	Inter- and intra-pulse	Calibration curve	4.55	3 ppbv detection limit 5 % for breath measurements as low as 140 ppbv	[6]
967.35 cm^{-1}	QCL	QEPAS WMS 2f	Reference cell	4.55	6 ppbv standard deviation for NH_3 in N_2 from 160 ppbv to 5 ppmv	[7]
1,103.44 cm^{-1}	QCL	Multi-pass cell WMS 2f/1f	Calibration free	0.98	7 ppbv detection limit 5 % total uncertainty for breath measurements	This work

QCL quantum cascade laser, *PAS* photo-acoustic spectroscopy, *CRDS* cavity ring down spectroscopy, *QEPAS* quartz enhanced photo-acoustic spectroscopy, *WMS* wavelength modulation spectroscopy

[a] Interference is defined as the contribution to the total absorbance at the ammonia peak from other species for a breath mixture at 100 Torr with 50 ppbv NH_3, assuming 6 % H_2O and 5 % CO_2. Note that the sensor developed in [1] did not list the specific ammonia feature so the interference could not be determined

[b] Detection limits were defined uniquely for each sensor, please refer to the references for more details
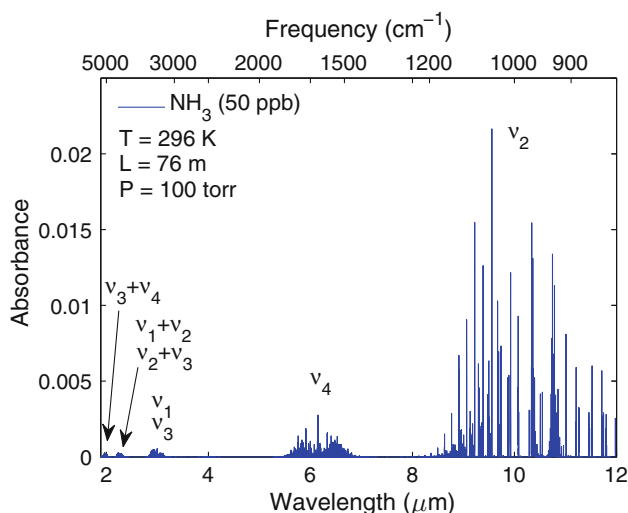

Fig. 1 Ammonia absorption from 2 to 12 μm showing the strongest absorbance in the v_2 vibrational band

cannot be predicted with the HITRAN broadening coefficients. Additionally, the six transitions that make up the ammonia manifold sR(6,K) near 1,103.44 cm^{-1} are listed in HITRAN with uncertainties between 10 and 20 %. Therefore, the development of this calibration-free sensor required the measurement of the linestrength and broadening coefficients of ammonia in nitrogen, oxygen, carbon dioxide, and water vapor for each of these six transitions, which was performed in our previous work [10].

2 WMS 2f/1f sensor implementation

Although direct absorption spectroscopy (DAS) is the simplest and most common technique to measure the mole

fraction of a species in a gas mixture with a laser-based sensor, the accurate detection of trace gases using DAS is challenging since low absorbance levels are difficult to distinguish from noise and the nonabsorbing baseline is uncertain. In order to measure the ppbv levels of ammonia found in breath, this sensor uses wavelength modulation spectroscopy (WMS), a well-known spectroscopic technique to make sensitive measurements and reject noise. In order to develop a calibration-free sensor, wavelength modulation spectroscopy with second harmonic normalized by first harmonic detection (WMS 2f/1f), as described previously by Rieker et al. [11] and Farooq et al. [12, 13], is used. The first harmonic normalization accounts for the opto-electrical gain of the system and losses due to scattering, beam stearing, and window fowling and eliminates the need for calibration.

In WMS, the laser frequency is modulated with angular frequency ω_m, by modulating the input current to the QCL, described by

$$v(t) = \bar{v} + a\cos(\omega_m t) \qquad (1)$$

where $\bar{v}$ (cm^{-1}) is the laser center frequency and a is the modulation depth. The intensity of the laser is modulated simultaneously according to

$$I_o(t) = \overline{I_o} + i_o\cos(\omega_m t + \psi_1) + i_2\cos(2\omega_m t + \psi_2) \qquad (2)$$

where $\overline{I_o}$ is the average laser intensity, i_o is the linear intensity modulation amplitude, ψ_1 is the linear phase shift, i_2 is the nonlinear intensity modulation amplitude, and ψ_2 is the nonlinear phase shift. Due to the higher order intensity modulation, there is a nonzero background signal in the absence of absorption.

The background-subtracted WMS 2f/1f signal is a function of both laser parameters (a, i_o, i_2, ψ_1, and ψ_2) and
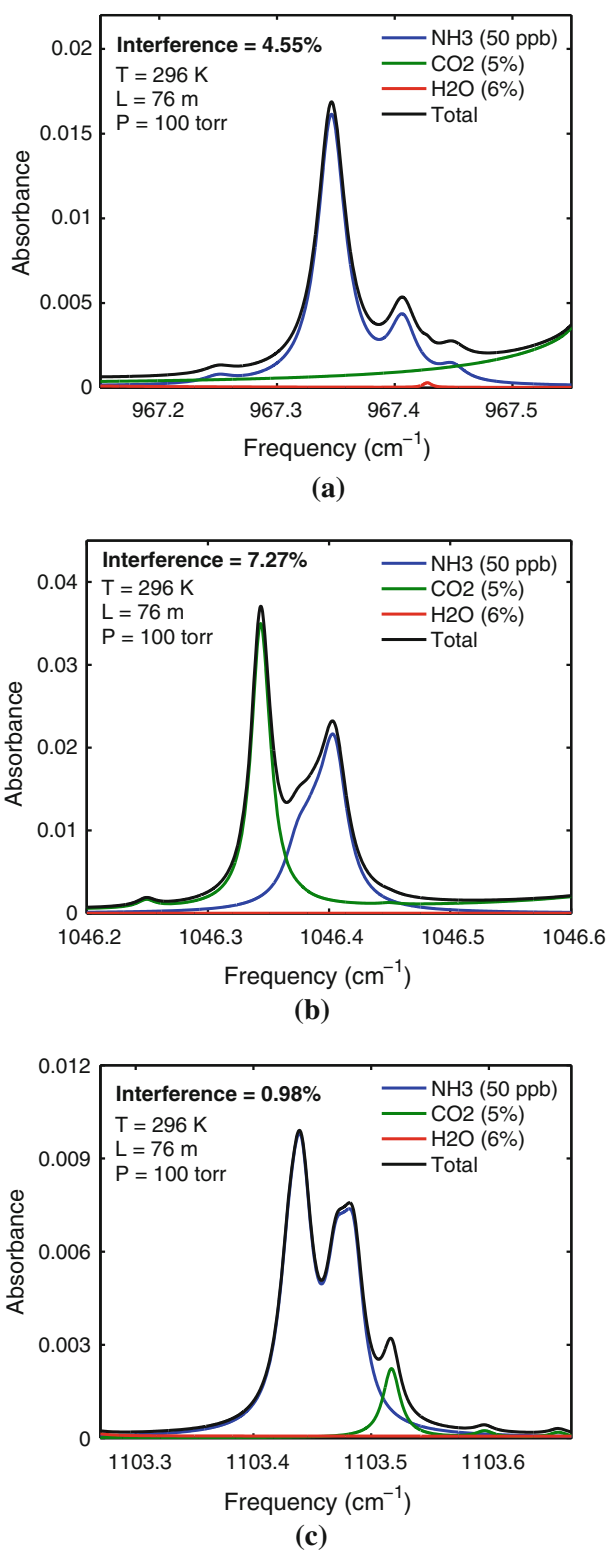
(a)

(b)

(c)

Fig. 2 Simulations of the interference from carbon dioxide (5 %) and water vapor (6 %) on low levels of ammonia (50 ppb), comparing the ammonia features used for previous sensors to the feature selected for this sensor. The interference, defined as (Total − NH$_3$)/Total absorbance at the ammonia peak, is lowest for the ammonia feature selected for this sensor. The spectrum for each individual species was calculated from parameters in HITRAN 2008 [8]. **a** Previous sensors [4, 6, 7] utilized the ammonia feature centered at 967.35 cm^{-1}. **b** A previous sensor [5] utilized the ammonia feature centered at 1,046.4 cm^{-1}. **c** This sensor utilizes the ammonia feature centered at 1,103.44 cm^{-1}

because it allows for the measurement of concentration without the need to calibrate the signal to a known mixture as is necessary with traditional WMS [11].

The laser parameters were measured for different laser settings (injection current, temperature, and wavelength) and over time. It was found that there was some variation in the exact values of the laser parameters from day to day, but the changes were negligible when using the sensor in a single day. Therefore, the laser parameters were measured each day before using the sensor to reduce the uncertainty in the measurement; typical values are given in Table 2.

With measurements of the pressure, temperature, and path length, the spectroscopic parameters determined previously [10], and the laser parameters, an in-house simulation code was used to calculate the WMS 2f/1f signal. The simulated background signal was found by running the simulation with ammonia mole fraction set to zero. A guessed ammonia mole fraction was then used to determine the simulated background-subtracted WMS 2f/1f signal and the peak value of this signal. The simulated peak value was used to calculate the actual mole fraction of ammonia by comparison with the measured peak value.

The measurements were performed using a continuous-wave quantum cascade laser (cw-QCL), model sbcw2006, from Alpes Lasers (Neuchâtel, Switzerland; http://www.alpeslasers.ch/), which was chosen since it is tunable over 1,100.4–1,108.2 cm^{-1} by adjusting the laser temperature and injection current. The laser temperature was varied using a TCU200 temperature controller supplied by Alpes Lasers, while the current was controlled using an ILX Lightwave LDX 3232 high compliance laser diode driver. The QCL was mounted in a laboratory laser housing, which included a thermoelectric cooler. Stronger absorbance levels were achieved by using an AMAC-76 astigmatic

gas parameters (P, T, L, S, ϕ, and X_i). The laser parameters can be determined before the measurements, according to the method described by Li et al. [14], and therefore, the sensor can be used to measure one of the gas parameters if others are known. This strategy is called "calibration free"

Table 2 Typical laser parameters at a modulation frequency of 10 kHz

a (cm^{-1})	$\frac{i_o}{I_o}$	$\frac{i_2}{I_o}$	ψ_1 (rad)	ψ_2 (rad)
0.067	0.291	0.007	3.36	5.40

multi-pass cell from Aerodyne Research [15, 16]. This optical cell has 238 laser passes, resulting in a total path length of 76.45 m. A ZnSe asphere was used to collimate the laser, and optics were used to focus the laser at the center of the cell with a focal ratio >f/80 to achieve optimal alignment. The laser was then directed to the Vigo PVI 3TE-10.6 thermoelectrically cooled, optically immersed photovoltaic detector where the intensity was recorded with a National Instruments data acquisition system (DAQ) NI PXIe-6115 sampling at 10 MHz with 12 bit resolution. The pressure was measured using MKS 627D capacitance manometers with 100 and 20 Torr full-scale pressure ranges and accuracies of 0.12 %. The breath samples were collected in SKC 239 Series Exhaled Breath Sample Bags, which have a volume of 1 l and are made of 4-ply low-background Flex Foil® PLUS material. The patient exhales into the breath bag through a valve, which is closed when breath acquisition is completed. The breath sample is extracted through the sample removal fitting and pumped through the optical cell for measurements at a pressure of 100 Torr and flow rate of 0.55 l per minute (lpm) with a Varian DS302 vacuum pump. The experimental setup is shown in Fig. 3.

To implement the WMS strategy, the laser frequency was set to the peak of the absorption, and the injection current was then modulated with a high frequency, 10 kHz, sine wave. An additional sinusoidal modulation with low frequency, 80 Hz, was added to the high frequency modulation so that the 2f/1f signal for a range of wavelengths could be determined. The purpose of this additional slow scan was to make sure the peak 2f/1f signal was captured. The resulting laser intensity, after having passed through the ammonia mixture in the multi-pass cell, was measured by the detector. The background signal was measured with pure nitrogen flowing through the cell. The measured background-subtracted 2f/1f is calculated from the individual components, which are processed using a digital lock-in filter and low-pass Butterworth filter to remove the high frequency noise and isolate the desired harmonics, as illustrated in [11].

The measured peak value, $C_{pk,meas}$, was then compared to the simulated peak value, $C_{pk,sim}$, to calculate the measured ammonia mole fraction.

$$X_{meas} = X_{guess} \frac{C_{pk,meas}}{C_{pk,sim}} \tag{3}$$

At low mole fractions, the simulated peak value is directly proportional to the guessed mole fraction so the first iteration is an accurate calculation of the measured mole fraction. For verification, though, the measured mole fraction was then used as the guessed mole fraction until the solution converged.

Figure 4 shows the output from the simulation for the first and second harmonic signals, the background-subtracted 2f/1f signal, and the region of the peak that was scanned during the measurement.

3 Sensor verification and analysis

3.1 Adsorption

Ammonia gas is known to adsorb strongly to surfaces it comes in contact with, and thus, the measured ammonia concentration in an optical cell decreases with time [17]. Large surface area and nonglass components, such as the mirrors, of the multi-pass cell provide more adsorption sites than the quartz cell, which was used for the spectroscopic measurements in our previous work [10]. Due to the adsorption in this optical cell, it was very difficult to study

Fig. 3 WMS 2f/1f sensor experimental setup used to measure ammonia mole fraction in breath as samples flow through a multi-pass cell
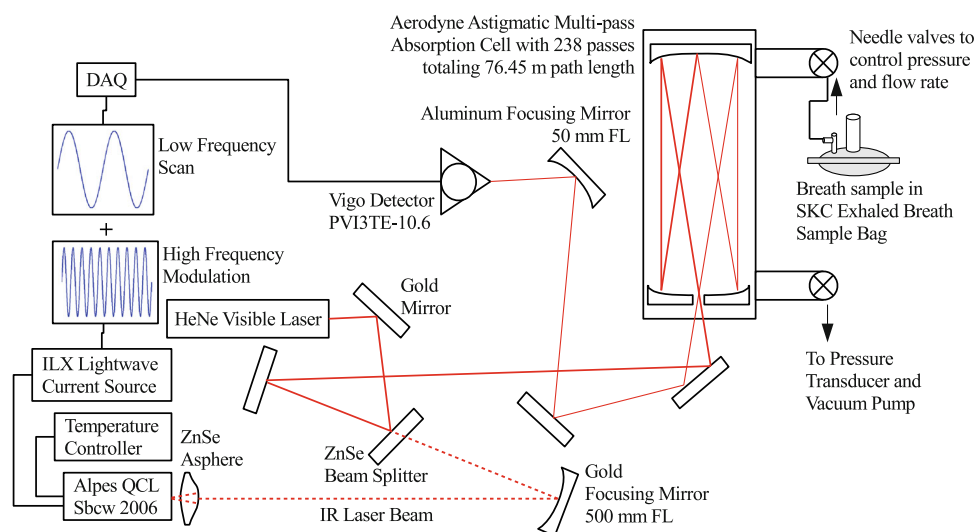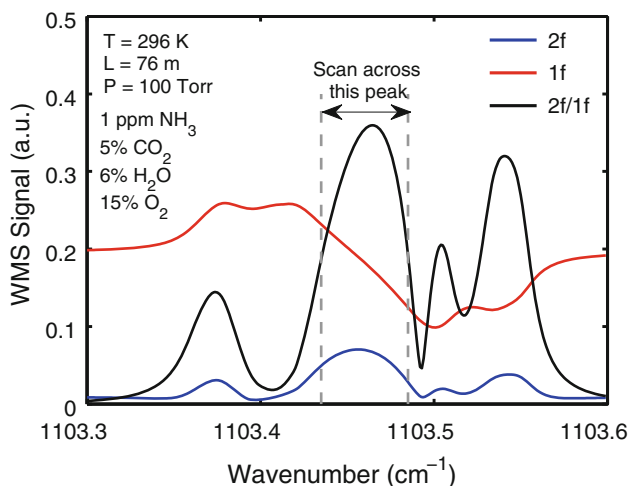
Fig. 4 Simulated WMS signals including the first and second harmonic signals as well as the background-subtracted 2f/1f signal showing the region of the slow scan

a static gas sample. Instead, a gas flow setup was used to minimize adsorption so the sensor measures the actual amount of ammonia in the gas sample. Since adsorption changes the amount of ammonia in the gas phase, it is important to quantify what effect it may have on the sensor performance.

Adsorption is an equilibrium process where the equilibrium gas phase concentration depends on three factors, the pressure, the temperature, and the tendency of the molecule to adsorb to the surface. For a given molecule and surface, the fraction of surface sites occupied by the adsorbed molecule increases with pressure and decreases with temperature [18, 19].

A detailed investigation of the effects of ammonia adsorption was performed previously for the design of an ammonia sensor based on photoacoustic spectroscopy (PAS) [17]. Since the adsorption process depends on the previous ammonia exposure in the cell, a closed cell will equilibrate to ammonia levels that are not reproducible and therefore cannot be corrected to calculate the actual value in the initial gas sample. In the case of a flow experiment, the adsorbed molecules can be replaced by new molecules entering the cell and molecules that desorb are carried out by the flow. Therefore, after a brief passivation delay [20], equilibrium conditions are reached and the effective adsorption rate decreases rapidly so the measured mole fraction of ammonia is in fact the mole fraction in the sample.

A series of validation tests were carried out to establish the optimal parameters required to reach equilibrium for the experimental setup used here. Ammonia mole fraction was measured as a function of time by flowing an ammonia–nitrogen mixture continuously through the cell. Figure 5 shows the results for four different tests. The first test

was performed after the cell was evacuated for 12 hours. Since the cell was initially far from equilibrium, the measured mole fraction continued to increase gradually and did not reach equilibrium during the test time. The second and third tests were performed afterward with only 10 min of evacuating the cell. For these tests, the mole fraction reached equilibrium faster since the cell started closer to equilibrium. The final test was performed with the cell heated to 35 °C, which resulted in a faster approach to equilibrium.

Additional validation tests were performed with pseudobreath mixtures from the sample breath bags. The bag was filled with ammonia, nitrogen, oxygen, carbon dioxide, and water vapor in amounts typical in breath. The primary difference between the ammonia–nitrogen mixture and the pseudobreath is that the latter also contains water vapor. Water vapor is another molecule, which tends to adsorb strongly. Also, ammonia tends to adsorb to water droplets which, if formed, could provide more adsorption sites. Therefore, the temperature and pressure in the cell were chosen such that the partial pressure of water vapor was below the vapor pressure so there would be no condensation of water in the cell.

Two sets of three experiments were performed with mixtures containing ammonia close to the higher and lower values expected in breath, respectively. It can be seen in Fig. 6 that in both cases, equilibrium was reached in the time provided by the limited volume of the bag. Additionally, the equilibrium value was repeatable within the measurement uncertainty. Ideal flow rates and pressures were achieved at room temperature using needle valves between the bag and the cell and between the cell and the vacuum pump. The pressure increased to 100 Torr in 40 s and then remained steady until the bag was empty, 70 s
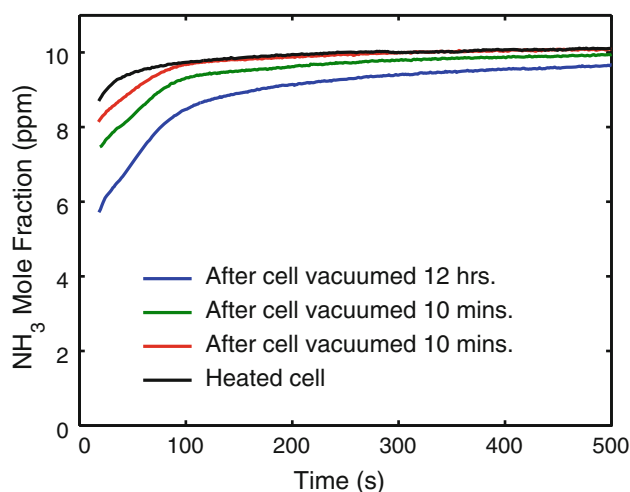

Fig. 5 Measurements of the time to reach equilibrium as a mixture of ammonia and nitrogen flowed through the cell for various cell conditions
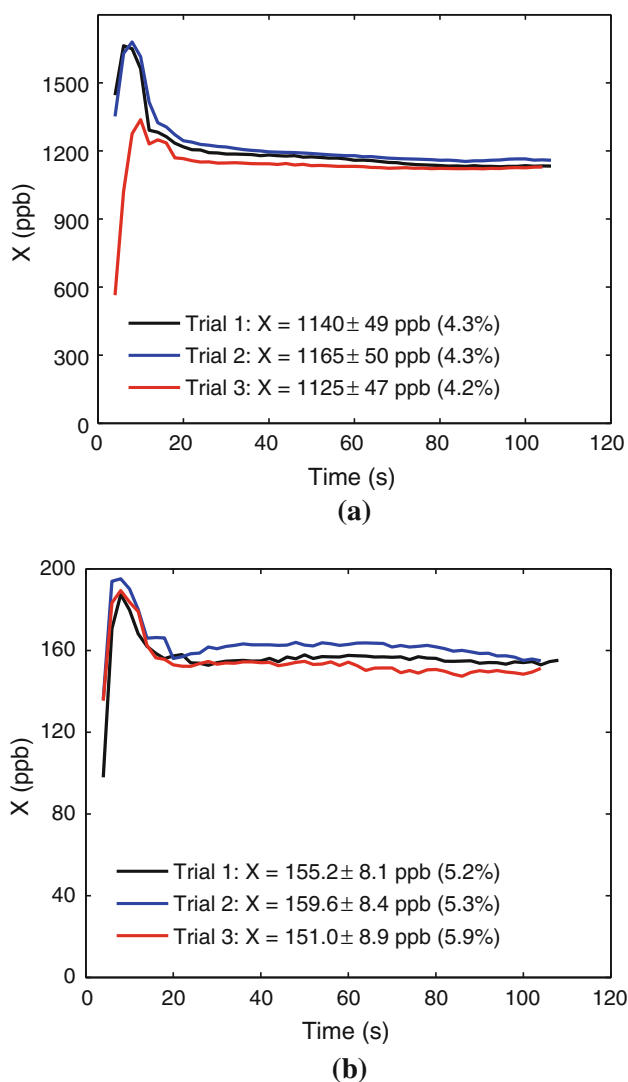
Fig. 6 Ammonia measurements in flow experiments; **a** ammonia near high values in typical breath, **b** ammonia near low values in typical breath

later. The flow rate was 0.55 lpm. The verification tests showed that this flow rate and sample volume are adequate to reach the equilibrium flow conditions.

The pseudobreath mixtures showed a different trend at early times compared to the ammonia–nitrogen mixtures. In ammonia–nitrogen mixtures (Fig. 5), the ammonia concentration increased steadily to an equilibrium value, whereas in pseudobreath mixtures (Fig. 6), ammonia concentration increased initially and then gradually decreased to the final equilibrium value. This is because the water vapor adsorption reaction competes with the ammonia adsorption reaction. The water molecules can replace ammonia on the adsorption sites and thus cause an initial net desorption of ammonia. Over time, with continuous flow, the equilibrium is re-established, and the ammonia level approaches the amount in the incoming sample.

3.2 WMS validation by DAS

Experiments were performed to compare results from direct absorption (DAS) and wavelength modulation (WMS) to validate the WMS strategy. The amount of ammonia was first measured in the cell for a flow experiment using WMS; next, the laser settings and modulation were changed to measure the amount of ammonia using DAS. Results for a mixture containing about 9.5 ppmv of ammonia are shown in Fig. 7, and the measured ammonia mole fraction by WMS clearly falls within the experimental uncertainty of the mole fraction measured by DAS. This experiment was repeated for more dilute mixtures to verify the sensor over a range of mole fractions, and the results are shown in Table 3. There were more scatter and uncertainty in the measurements with DAS, especially at ammonia levels below 1 ppmv, which is why WMS was used for this sensor.

3.3 WMS simulation sensitivity analysis

Since the measured peak signal is compared with the simulated peak to infer the ammonia mole fraction, it is important to quantify the sensitivity of the simulated peak value to the spectroscopic parameters, the gas properties, and the laser parameters.

In previous work [10], the linestrength and collisional broadening coefficients for ammonia in nitrogen, oxygen, carbon dioxide, and water vapor were measured. The uncertainty on measured linestrength values ranged from 6 to 10 %, while the uncertainty on measured collisional broadening coefficients ranged from 3 to 13 %. Simulations were performed in which one of the parameters was adjusted by its uncertainty, while the others were
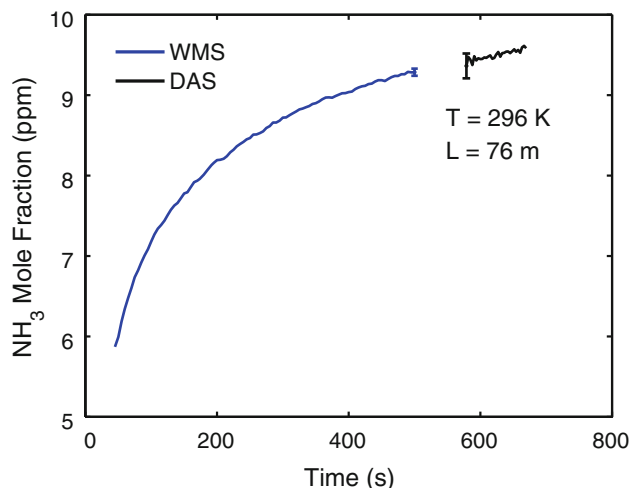

Fig. 7 Comparison between WMS and DAS for an ammonia mixture in nitrogen

Table 3 Comparison between ammonia mole fraction measured with WMS and DAS used to validate the WMS method

WMS	DAS	
9.28	9.36	ppmv
6.85	6.90	ppmv
5.95	6.05	ppmv
2.21	2.20	ppmv
124	122	ppbv
50	43	ppbv

maintained at their measured value. The resulting WMS peak value was compared with the peak value for the simulation with all of the parameters at their measured value. Figure 8 shows the effect of the uncertainty of the linestrength for each of the six ammonia transitions that make up the sR(6,K) manifold near 1,103.44 cm^{-1}. Transition sR(6,3) is the strongest and the closest to the frequency of the peak WMS signal, so the simulated peak signal has largest sensitivity (2.31 % change) to this transition. The peak signal has less sensitivity to the linestrength of other ammonia transitions as they are further away from the peak and have relatively small linestrength. The same analysis was used to study the effect of the uncertainty of the collisional broadening coefficients for each of the bath gases. The WMS peak was most sensitive to nitrogen broadening, since it is the most abundant ($\sim$74 %) bath gas in breath, which led to an uncertainty of 1.68 % in the simulated peak value.

The concentrations of the other gases in breath were not simultaneously measured, since the interference absorption leads to a relatively small uncertainty. Exhaled breath typically has 6 % water vapor and between 3 and 6 % carbon dioxide [21]. At the measurement wavelength, the water vapor interference was negligible and the carbon dioxide interference was only apparent for ammonia mole fractions <1 ppmv. The WMS simulation was designed to subtract the interference absorption by assuming a concentration of carbon dioxide. At a pressure of 100 Torr and ammonia mole fraction of 200 ppb, the ammonia WMS peak changed 1 % for carbon dioxide concentrations between 3 and 6 %. The uncertainty in the relative amounts of bath gases also affected the ammonia signal because the bath gas concentrations are included in the calculation of collisional linewidth. At a pressure of 100 Torr, a change in the amount of water vapor by 1 % resulted in a change in the peak value by 0.84 %, while a change in the amount of carbon dioxide by 3 % resulted in a change in the peak value by 0.62 %, and a change in the amount of oxygen by 3 % resulted in a change in the peak value by 0.43 %. Since the nitrogen makes up the remainder of the mixture in the simulations, the effect of changing the amount of nitrogen is accounted for in the above calculations.

The temperature of the gas in the cell was assumed to be room temperature, which was measured to be between 294 and 296 K. This 2 K difference led to 0.38 % change in the simulated WMS peak value. The pressure in the cell during experiments was measured with an MKS manometer that has a reported uncertainty of 0.12 %. Additionally, a slight variation in pressure was observed as the flow reached equilibrium conditions. The total uncertainty in the measured pressure was 0.5 %, which led to a change in the simulated peak of 0.31 %. The manufacturer reported a cell path length of 76.45 ± 0.05 m which was confirmed, within experimental error, by measuring an ethylene absorption line. This uncertainty in the path length led to a change in the simulated peak of 0.07 %. As described in Sect. 2, implementation of calibration-free WMS requires laser-specific modulation parameters (i_0, i_2, ψ_1, ψ_2). These were measured each day to account for small variations from day to day. The uncertainty in the experimentally determined laser parameters led to a change in the simulated WMS peak of 0.8 %.

The overall sensitivity analysis, shown in Fig. 9, reveals that the most significant input parameters to the simulation program are the linestrength of transition sR(6,3) and the collisional broadening coefficients for ammonia in nitrogen. Based on this analysis, the total uncertainty in the simulated WMS peak value, $\sigma_{C_{pk,sim}}$, was found by combining the uncertainties of all input parameters, i, using the Euclidean norm

$$\sigma_{C_{pk,sim}} = \sqrt{\sum_i \sigma_i^2} \qquad (4)$$

where σ_i denotes the percent change in the simulated WMS peak due to the uncertainty in parameter i. For ammonia mole fractions <1 ppmv, when the effect of carbon dioxide interference was included, the uncertainty in the simulated peak was found to be 4.05 %. For ammonia levels above 1 ppmv, the uncertainty was found to be 3.92 %. Since the measured mole fraction is proportional to the simulated WMS peak value, this uncertainty is the contribution from the simulation to the measured mole fraction. This simulation uncertainty is then combined with the experimental uncertainty to determine the overall uncertainty of the measured mole fraction.

3.4 Detection limit

To quantify the sensor's detection limit and sensitivity, an experiment was performed where ammonia concentration was varied continuously. Figure 10a shows the results for this experiment. Initially, pure nitrogen was measured, then a 9 ppmv ammonia in nitrogen mixture was added at a slowly increasing fractional flow rate, and then, the ammonia mixture was turned off so that pure nitrogen

Fig. 8 Comparing simulated WMS 2f/1f peak for measured linestrengths to the simulation when each linestrength is changed by its uncertainty
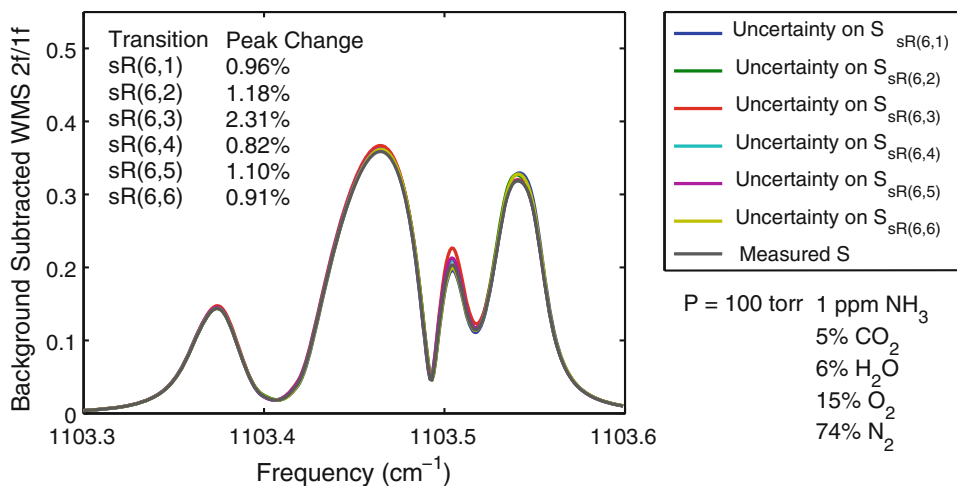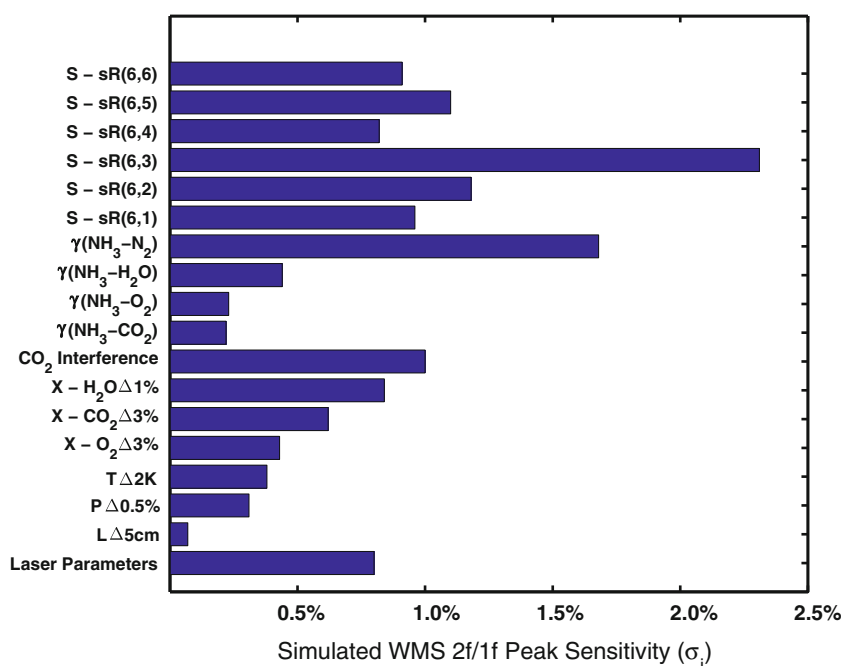

Fig. 9 Effect of the input parameters' uncertainty on the simulated WMS 2f/1f peak

flowed through the cell again. It can be seen that the measured amount of ammonia slowly increased as more ammonia was added to the flow and then quickly decreases to a small amount of residual ammonia as the cell was flushed with nitrogen. Figure 10b zooms in to the initial rise of ammonia mole fraction.

The sensor measured an ammonia mole fraction of about 7 ppbv when pure nitrogen flowed through the cell; this erroneous measurement was not due to ammonia absorption, but due to fluctuations in the background signal. The background signal used for this experiment was the average of 10 measurements with pure nitrogen flowing through the cell. Figure 11a shows how the measurement of pure nitrogen gives a nonzero peak value after background subtraction. The detection limit is then 7 ± 2 ppbv, approximately.

After the addition of the ammonia mixture, peaks began to become distinct from the background signal, as seen in Fig. 11b. The peak value used to determine the ammonia mole fraction was the average of fifteen peaks, and six are shown in the figure. The measurement uncertainty was defined as the standard deviation in these fifteen peak values. The uncertainty in the peak value at a measured ammonia mole fraction of 18.3 ppbv was 18.2 %. Combining this uncertainty with the uncertainty in the simulated WMS peak, using the Euclidean norm, led to a total uncertainty of 18.6 % or 3.4 ppbv.

Since this sensor was designed to measure the amount of ammonia in exhaled breath, it was important to quantify the sensitivity near expected values in breath. Healthy patients are expected to have anywhere from 100 to 500
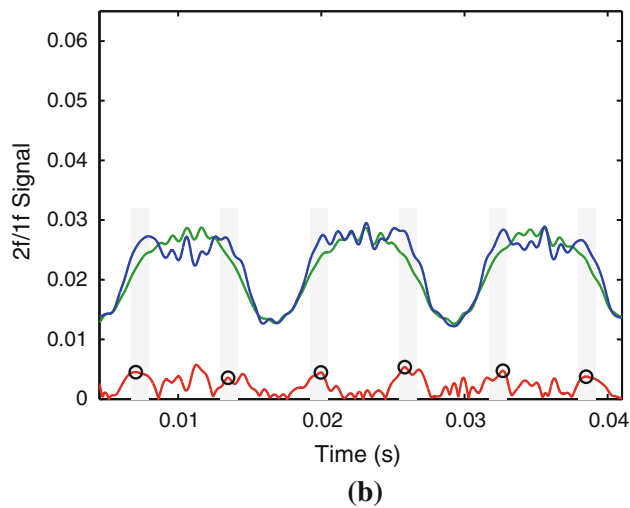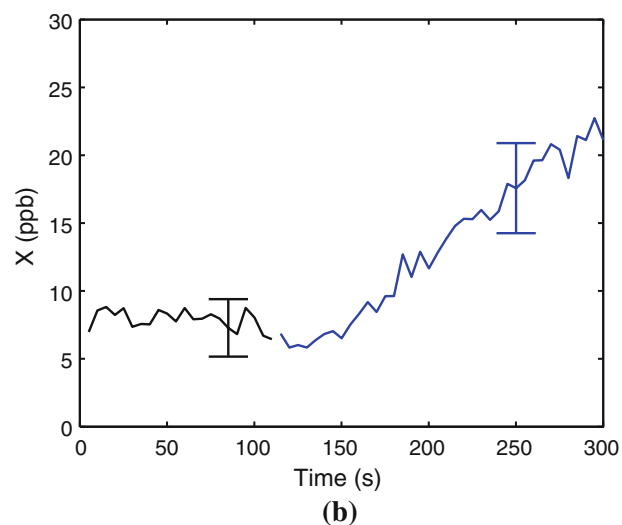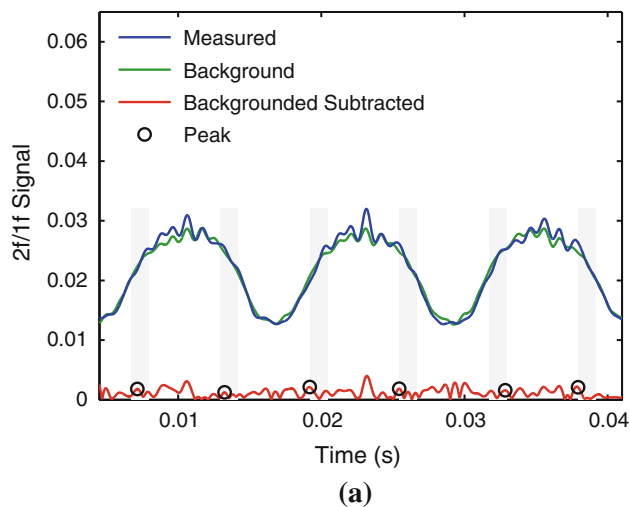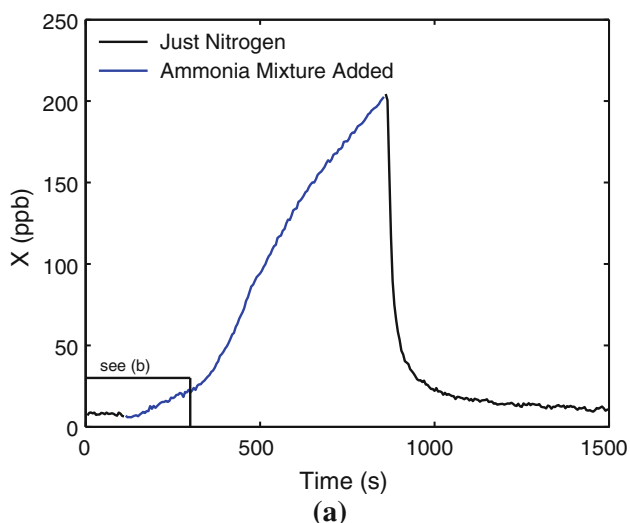
Fig. 10 Characterization of the sensor using WMS to measure low levels of ammonia. **a** Entire measurement. **b** Initial ammonia addition

ppbv ammonia, while patients with CKD are expected to have >1 ppmv ammonia. Figure 11c shows the signal for a measurement of 154.6 ppbv. In this case, the peaks are clearly distinguishable from the background signal. The measurement uncertainty was found to be 2.1 % leading to a total uncertainty of 4.58 % or 7.1 ppbv.

4 Results from breath measurements

4.1 Real-time measurement of breath samples from healthy patients

The sensor was implemented to study the ammonia concentration in the exhaled breath of healthy individuals. Measurements were taken in real time with the breath
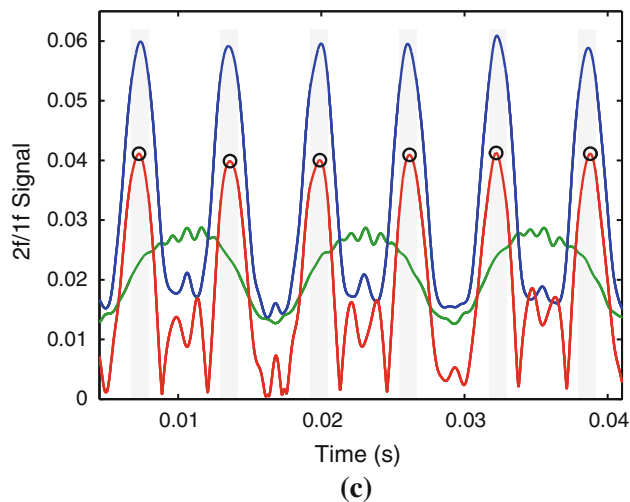

Fig. 11 WMS 2f/1f results for **a** pure N_2, **b** after the initial addition of ammonia, and **c** once the ammonia amount reached typical levels in breath. **a** Measurement of 7.3 ± 2.1 ppbv. **b** Measurement of 18.3 ± 3.4 ppbv. **c** Measurement of 154.6 ± 7.1 ppbv

sample bag as a buffer volume. Figure 12 shows three examples of the measurements of breath samples from different healthy patients. The first 60 s shows the measurement when pure nitrogen was flowing through the cell, after which the patient exhaled into the bag and the sensor measured the ammonia in the breath. Experiments were done previously to verify that the flow rate was sufficiently high to replace the nitrogen in the cell by the incoming sample. Therefore, the initial rise in mole fraction is over the time it takes for the breath sample to completely fill the cell and for the nitrogen to be removed. Thereafter, the breath flow continues as equilibrium is established until the bag is empty.

Ammonia concentration was measured in the exhaled breath of eight different healthy patients. The reported ammonia level is the average value measured over the last 10 s before the sample was consumed. The reported uncertainty accounts for the uncertainty in the simulated WMS peak, as described previously, and the standard deviation over the measurement time. Figure 13 shows the results for these eight patients, all of which were between 100 and 350 ppbv, within the expected range for healthy patients. The amount of ammonia in the exhaled breath of one healthy patient over the course of the afternoon was also measured. Figure 14 shows that the amount of ammonia decreased after a meal, then increased steadily between meals, and again decreased after another meal. This is in agreement with results from previous work [4]. The amount of ammonia was within the expected range except long after one meal when it was above 500 ppbv.

4.2 Measurement of breath samples from patients diagnosed with Chronic Kidney Disease (CKD)

Breath samples were collected in the breath sample bags from patients diagnosed with CKD. The bags were then
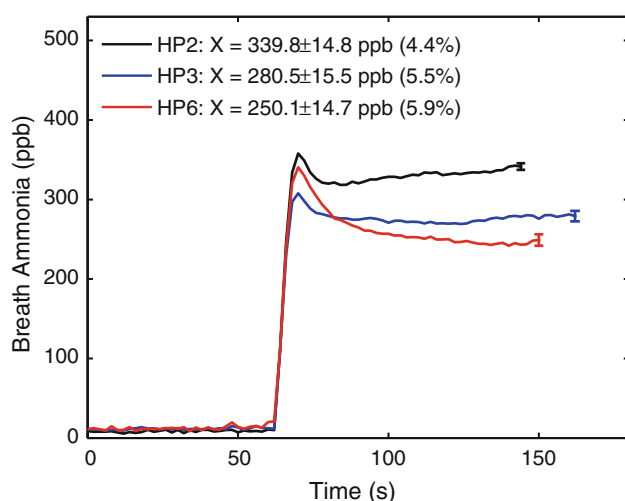

Fig. 12 Measurement of breath samples from three healthy patients after 1 min of nitrogen flow from the sample bag
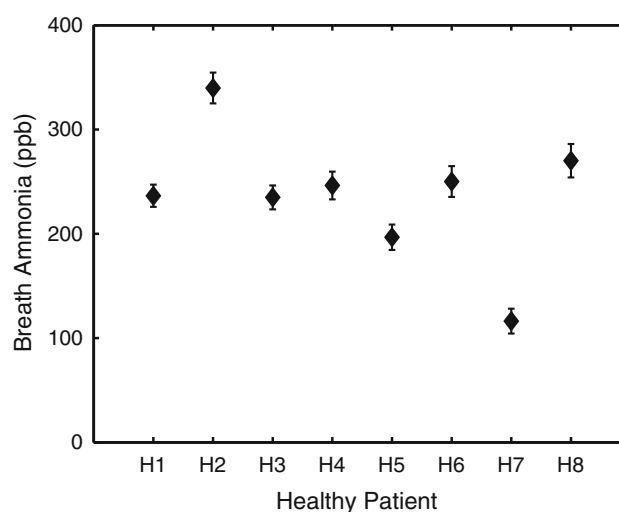

Fig. 13 Results from eight healthy patients including male and female, smokers and nonsmokers, between the ages of 18 and 50

transported to the research facility for the analysis of patient breath. These bags are specifically designed for collecting and storing human breath samples. A study was done previously to investigate the suitability of the bag material for storing atmospheric samples containing ammonia. The results showed that 100 % of the ammonia was recovered after 2 h and over 90 % of the ammonia was recovered after 6 h [22]. The study also recommended a procedure for cleaning the bags to make them suitable for reuse. The cleaning procedure involved emptying the bag, flushing it with room air, filling it with zero air for 24 h, emptying it, then refilling it with zero air again to measure the residual gas concentrations. Following this procedure, the bags were found to have <25 ppbv residual ammonia. Another study investigating the bags for breath research recommended heating the bags to 45 °C as part of the cleaning procedure [23].

To verify that the bags were suitable for storing the breath samples, an experiment was designed to measure the amount of ammonia in the bag overtime. Since the full volume of the bag was required for each measurement, three bags were filled with the same pseudobreath mixture simultaneously. The amount of ammonia in consecutive bags was measured immediately after filling, 2 1/2 h after filling, and 31/2 h after filling. These experiments were performed for two different initial ammonia mole fractions. The results, listed in Table 4, show that a substantial portion of ammonia was lost overtime.

These losses are likely due to the ammonia molecules adsorbing to surfaces of the sample bag. The different behavior between these conditions and the ones in the previous research investigating the bags [22] is likely due to the water content, which is much larger in a breath sample compared to an atmospheric air sample. The
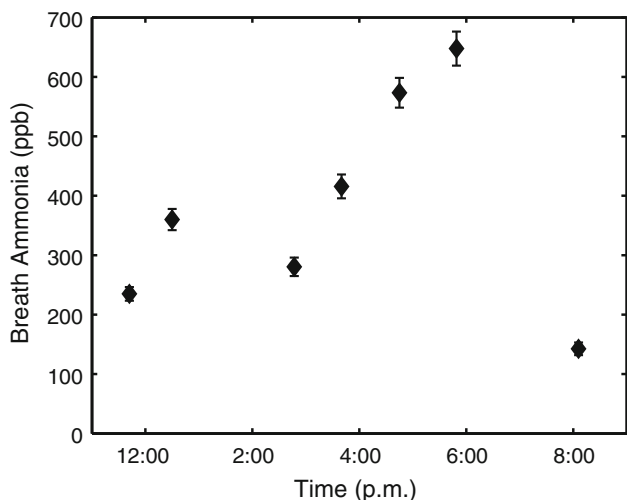
Fig. 14 Results for one healthy patient throughout the day, where the lunch meal was at 1:30 p.m. and the dinner meal was at 7:00 p.m.

Table 4 Percent remaining at 2½ and 3½ h for each of the initial mixtures

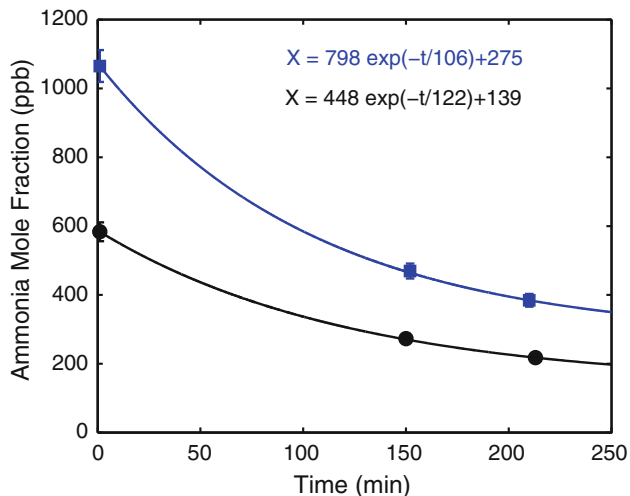| X_{initial} (ppbv)	585 (%)	1,073 (%)
$\frac{X(2\frac{1}{2}\,h)}{X_{\text{initial}}}$	46	44
$\frac{X(3\frac{1}{2}\,h)}{X_{\text{initial}}}$	37	36

Fig. 15 Results listed in Table 4 are fit with an exponential decay correlation

presence of saturated water can contribute to the losses of gas phase ammonia molecules.

The results from the verification experiments were used to develop a correlation to calculate the initial amount of ammonia in the breath sample based on the measured amount and the time between the sample acquisition and the measurement. To develop this correlation, the results
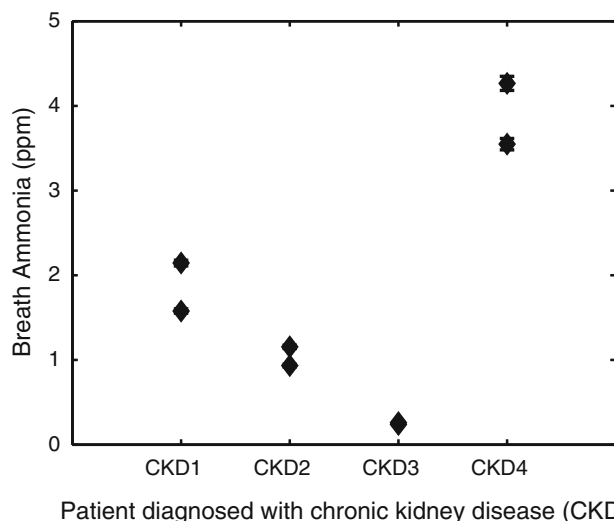

Fig. 16 Breath ammonia results from four patients diagnosed with CKD

listed in Table 4 were fit with an exponential decay function, as can be seen in Fig. 15, of the form:

$$X = \left(X_o - X_{\text{eqb}}\right) \exp(-t/\tau) + X_{\text{eqb}} \qquad (5)$$

According to the Langmuir [18], at low concentrations of ammonia, the equilibrium amount of ammonia, X_{eqb}, in the gas phase is linearly proportional to the initial amount of ammonia, X_o, in the gas phase. These two experiments were used to determine this linear relationship. Using the average decay time constant, τ, the developed correlation was used to determine the initial ammonia mole fraction from a single measurement of the ammonia mole fraction carried out at a later time after collection of the breath sample in the breath bag.

For ammonia measurements in the breath samples of CKD patients, the cell was evacuated before the breath sample flowed through the cell and equilibrium was reached before the sample was depleted. Two samples from four different patients were collected and analyzed. Figure 16 shows that each patient had significantly different amounts of ammonia in his/her breath. Patients CKD1, 2, and 4 had levels in the expected range for patients diagnosed with CKD, while patient CKD3 had levels in same range as expected for healthy patients.

Patients are diagnosed with CKD when their kidneys do not properly filter their blood, resulting in the accumulation of toxins in their blood, one of which is urea. Ammonia is part of the urea cycle and will therefore likewise accumulate in the blood. Ammonia can diffuse out of the blood into the lungs when the ammonia levels become higher than the ammonia levels in the inhaled air [24]. The relationship between breath ammonia and blood urea makes an ammonia breath sensor a potential diagnostic and
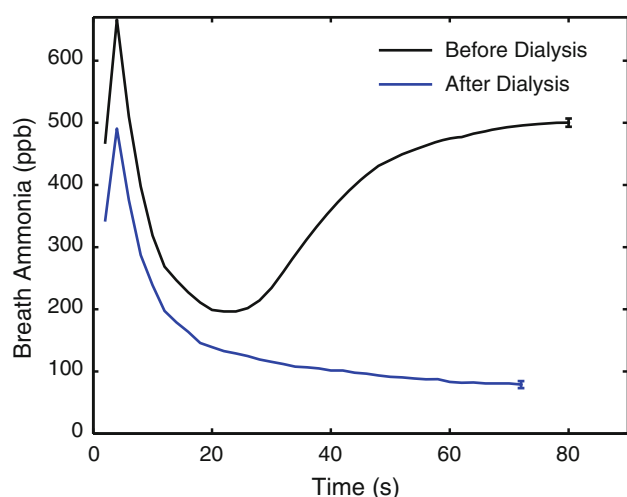
Fig. 17 Measurement of the breath ammonia for patient CKD2 from samples taken before and after the dialysis treatment
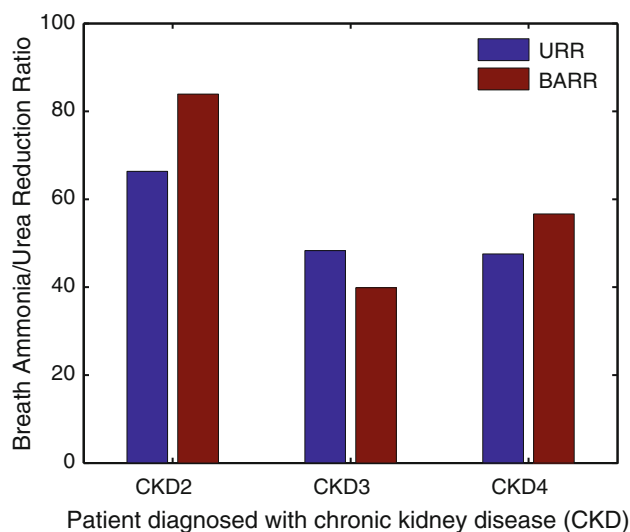

Fig. 18 Comparison between the urea reduction ratio (URR) and breath ammonia reduction ratio (BARR), used to test the adequacy of the dialysis treatment, for three patients diagnosed with CKD

monitoring tool for CKD. Patients with CKD are treated by dialysis on a regular basis to filter their blood. As a result of the filtering, the urea in the blood decreases during dialysis. The adequacy of dialysis is measured with the urea reduction ratio (URR), which is the percent decrease in blood urea nitrogen (BUN).

$$URR = \left(\frac{BUN_{\text{Before Dialysis}} - BUN_{\text{After Dialysis}}}{BUN_{\text{Before Dialysis}}} \right) \quad (6)$$

To compare the relationship between breath ammonia and blood urea, a breath ammonia reduction ratio (BARR) can be calculated to determine the percent decrease in breath ammonia [1].

$$BARR = \left(\frac{X_{\text{Before Dialysis}} - X_{\text{After Dialysis}}}{X_{\text{Before Dialysis}}} \right) \quad (7)$$

Figure 17 shows the measurements of the breath samples from patient CKD2 taken before and after the dialysis treatment. Blood tests were performed for patients CKD2, 3, and 4, so a comparison between the URR and BARR was made, as shown in Fig. 18. For each patient, a decrease in the BUN was accompanied by a decrease in the breath ammonia level. Dialysis is considered successful when the URR is >65 % [1]. While the BARR and URR are somewhat different, they do give the same qualitative measure of adequacy. It is expected that the breath ammonia sensing can, in future, replace the need to do regular blood tests.

5 Conclusions

A calibration-free sensor was designed to measure ppbv levels of ammonia in exhaled breath using a quantum cascade laser and a multi-pass cell. The ammonia absorption feature near $1,103.44 \text{ cm}^{-1}$ was selected due to its strong absorption and minimal interference from carbon dioxide and water vapor. WMS 2f/1f was implemented to improve the signal-to-noise ratio and the accuracy of measurements. The adsorption of ammonia in the cell was overcome by gas flow at 0.55 lpm and at a pressure of 100 Torr. The minimum detectable ammonia mole fraction was found to be 7 ppbv. The uncertainty from the WMS 2f/1f simulation based on the uncertainties in the input parameters was 4.05 % leading to a total uncertainty of 5 % for breath measurements.

This work demonstrated successful implementation in measuring ammonia levels immediately after the patient exhaled into the sample breath bag. For healthy patients, it was found that ammonia levels vary between individuals within the expected range and that ammonia levels vary for the same person depending on the meal time. Qualitatively, most patients with CKD had elevated levels of ammonia compared to healthy patients, and all of the patients showed a decrease in breath ammonia during dialysis.

References

1. L. Narasimhan, W. Goodman, C. Patel, Correlation of breath ammonia with blood urea nitrogen and creatinine during hemodialysis. Proc. Nat. Acad. Sci. **98**, 4617 (2001)

2. D. Kearney, T. Hubbard, D. Putnam, Breath ammonia measurement in helicobacter pylori infection. Dig. Dis. Sci. **47**, 2523–2530 (2002)
3. H. Wakabayashi, Y. Kuwabara, H. Murata, K. Kobashi, A. Watanabe, Measurement of the expiratory ammonia concentration and its clinical significance. Metab. Brain Dis. **12**, 161–169 (1997)
4. J. Manne, O. Sukhorukov, W. Jäger, J. Tulip, Pulsed quantum cascade laser-based cavity ring-down spectroscopy for ammonia detection in breath. Appl. Opt. **45**, 9230–9237 (2006)
5. Y. Bakhirkin, A. Kosterev, G. Wysocki, F. Tittel, T. Risby, J. Bruno, Quantum cascade laser-based sensor platform for ammonia detection in exhaled human breath, in *Laser Applications to Chemical, Security and Environmental Analysis*, St. Petersburg, Florida, (Optical Society of America, Washington, DC, 2008)
6. J. Manne, W. Jäger, J. Tulip, Sensitive detection of ammonia and ethylene with a pulsed quantum cascade laser using intra and interpulse spectroscopic techniques. Appl. Phys. B **94**(2), 337–344 (2009)
7. R. Lewicki, A. Kosterev, D. Thomazy, T. Risby, S. Solga, T. Schwartz, F. Tittel, Real time ammonia detection in exhaled human breath using a distributed feedback quantum cascade laser based sensor, in *Proceedings of SPIE*, vol. 7945 (2011), pp. 79450K-1–79450K-7
8. L.S. Rothman, I.E. Gordon, A. Barbe, D.C. Benner, P.F. Bernath, M. Birk, V. Boudon, L.R. Brown, A. Campargue, J.-P. Champion et al., The HITRAN 2008 molecular spectroscopic database. J. Quant. Spectrosc. Radiat. Transf. **110**, 533–572 (2009)
9. K. Sun, L. Tao, D. J. Miller, M. A. Khan, M. A. Zondlo, Inline multi-harmonic calibration method for open-path atmospheric ammonia measurements. Appl. Phys. B **110**(2), 213–222 (2012)
10. K. Owen, Et. Es-sebbar, A. Farooq, Measurements of NH_3 linestrengths and collisional broadening coefficients in N_2, O_2, CO_2, H_2O near 1103.46 cm^{-1}. J. Quant. Spectrosc. Radiat. Transf. **121**, 56–68 (2013)
11. G. Rieker, J. Jeffries, R. Hanson, Calibration-free wavelength-modulation spectroscopy for measurements of gas temperature and concentration in harsh environments. Appl. Opt. **48**, 5546–5560 (2009)
12. A. Farooq, J. Jeffries, R. Hanson, Sensitive detection of temperature behind reflected shock waves using wavelength modulation spectroscopy of CO_2 near 2.7μm. Appl. Phys. B Lasers Opt. **96**, 161–173 (2009)
13. A. Farooq, J. Jeffries, R. Hanson, Measurements of CO_2 concentration and temperature at high pressures using 1f-normalized wavelength modulation spectroscopy with second harmonic detection near 2.7 μm. Appl. Opt. **48**, 6740–6753 (2009)
14. H. Li, G. Rieker, X. Liu, J. Jeffries, R. Hanson, Extension of wavelength-modulation spectroscopy to large modulation depth for diode laser absorption measurements in high-pressure gases. Appl. Opt. **45**, 1052–1061 (2006)
15. J. McManus, P. Kebabian, M. Zahniser, Astigmatic mirror multipass absorption cells for long-path-length spectroscopy. Appl. Opt. **34**, 3336–3348 (1995)
16. J. McManus, M. Zahniser, D. Nelson, Dual quantum cascade laser trace gas instrument with astigmatic herriott cell at high pass number. Appl. Opt. **50**, A74–A85 (2011)
17. A. Schmohl, A. Miklos, P. Hess, Effects of adsorption-desorption processes on the response time and accuracy of photoacoustic detection of ammonia. Appl. Opt. **40**, 2571–2578 (2001)
18. I. Langmuir, The constitution and fundamental properties of solids and liquids. part i. solids. J. Am. Chem. Soc. **38**, 2221–2295 (1916)
19. S. Brunauer, P. Emmett, E. Teller, Adsorption of gases in multimolecular layers. J. Am. Chem. Soc. **60**, 309–319 (1938)
20. R. Yokelson, T. Christian, I. Bertschi, W. Hao, Evaluation of adsorption effects on measurements of ammonia, acetic acid, and methanol. J. Geophys. Res. **108**, 4649 (2003)
21. D. Smith, A. Pysanenko, P. Španěl, The quantification of carbon dioxide in humid air and exhaled breath by selected ion flow tube mass spectrometry. Rapid Commun. Mass Spectrom. **23**, 1419–1425 (2009)
22. N. Akdeniz, K. Janni, L. Jacobson, B. Hetchler, Comparison of gas sampling bags to temporarily store hydrogen sulfide, ammonia, and greenhouse gases. Trans. ASABE **54**, 653–661 (2011)
23. P. Mochalski, B. Wzorek, I. Sliwka, A. Amann, Suitability of different polymer bags for storage of volatile sulphur compounds relevant to breath analysis. J. Chromatogr. B **877**, 189–196 (2009)
24. B. Timmer, W. Olthuis, A. Berg, Ammonia sensors and their applications a review. Sens. Actuators B Chem. **107**, 666–677 (2005)